SM 1. Image analysis

The image processing program includes 3 main parts, the details are described as follows:

(i) Before executing edge detection, a Gaussian filter with a standard deviation (σ) of 4 and a 5 × 5 kernel is employed on the raw TIFF image for smoothing and removing noises. Subsequently, the Canny edge detector is employed to identify the drop boundary. The upper threshold is established using Otsu's method to initiate the edge selection, while the lower threshold is set at half of the upper threshold.

(ii) After the collection of pixels representing the drop boundary, we proceed to identify the coordinates of contact point using the so called profile method (Kalantarian *et al.* 2011). First, the substrate position is determined by averaging the vertical coordinates of a set of pixels that are vertically aligned near the contact point. This is based on the symmetry between drop profile and its reflection. Then a linear fitting process is conducted using 20 pixels, and the extrapolated point lying between the fitted straight line and the substrate line is identified as the contact point.

(iii) The high-speed camera captures images with a resolution of 1024×768 pixels. The utilization of a 5x magnification lens enhances resolution but, concurrently, narrows the global observation of the drop. With the zoom lens, each pixel represents a length of 3 μm, resulting in an actual field of view of 3.1×2.3 mm^2. This setup, while limiting the complete capture of a 10 μL droplet with a diameter of approximately 2.7mm, prompts the need for local analysis rather than global fitting to extract the contact angle.

Despite this limitation, the local drop profile can be considered as a continuous function over a closed and bounded interval. According to the Weierstrass approximation theorem, we approximate the drop profile by a polynomial. Notably, polynomial fitting in the polar coordinate system (PPF) is found to be more suitable, especially near 90°, than Cartesian coordinate system fitting (Atefi *et al.* 2013). Given that drop deformation during oscillation results in dynamic contact angles ranging from 70° to 120°, polar polynomial fitting emerges as a better option for our experiment. Prior to fitting, we transform the drop boundary into the polar coordinate system. The polynomial can be expressed as:

$$r(\varphi) = \sum_{n=0}^{N} a_n \varphi^n, \tag{SM 1.1}$$

where (r, φ) represents the polar coordinates. The correlation between the Cartesian coordinates (x, y) and polar coordinates is:

$$y = r \sin\varphi, x = r \cos\varphi. \tag{SM 1.2}$$

The subsequent question is how to choose appropriate order and number of pixels for the fitting procedure. To determine the optimal order of polynomial and number of pixels for fitting, a comparison is conducted across various polynomial orders and pixel numbers, checked with three distinct drop configurations, as shown in figure SM 1. Higher order polynomials require more pixel for fitting to reach a stable region. We use correlation coefficient (R^2) to evaluate the fitting accuracy, as shown in figure SM 2.

Finally, the contact angle is estimated as:

$$\theta = \arctan\left(\frac{r' \sin\varphi + r\cos\varphi}{r'\cos\varphi - r\sin\varphi}\right). \tag{SM 1.3}$$

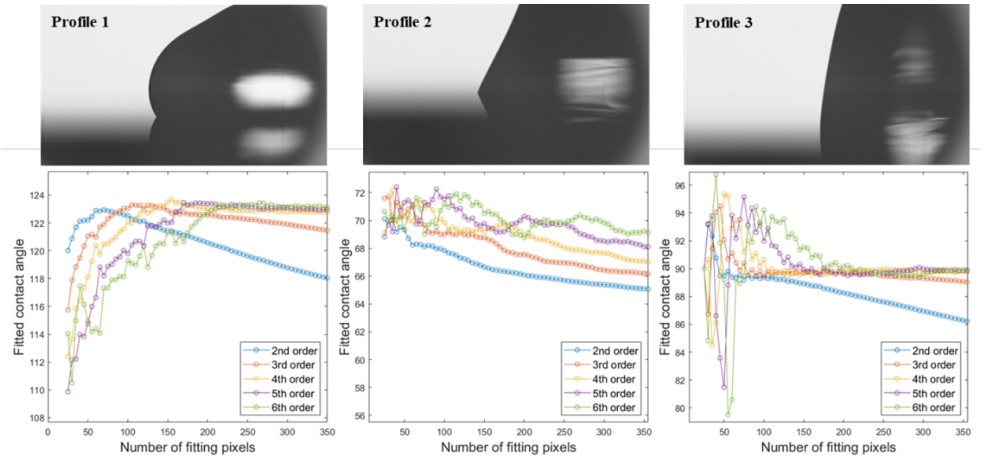

Figure SM 1: The comparison between the fitted contact angle with various order of polynomials.

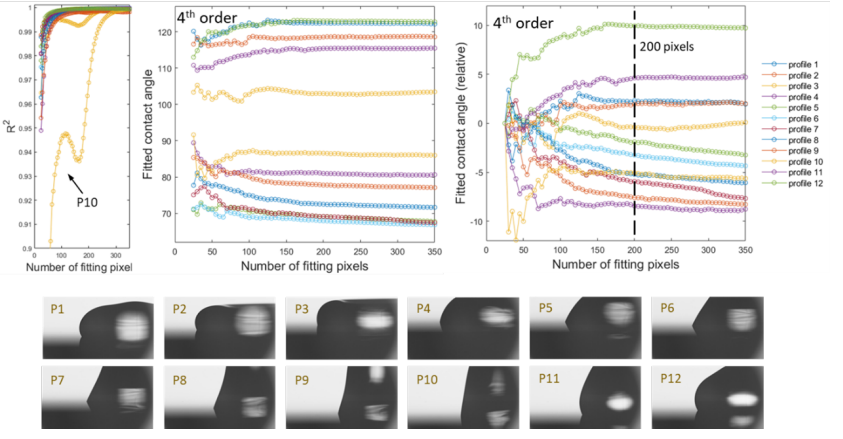

Figure SM 2: The comparison between the fitted contact angle with different number of pixels using 4^{th} order polynomial fitting. 200 pixels are found to be a safe choice for the fitted contact angles of all the profiles to reach a stable region.

SM 2. Relationship between the dynamic contact angle and contact line acceleration

In figure SM 3 we depict the relationships between θ_d and contact line acceleration $\dot{U}$ across various substrates. The curves exhibit a distinct pattern, resembling the contour of a bold letter 'z'.

REFERENCES

Atefi, E., Mann Jr, J. A. & Tavana, H. 2013 A robust polynomial fitting approach for contact angle measurements. *Langmuir* **29** (19), 5677–5688.

Kalantarian, A., David, R., Chen, J. & Neumann, A. W. 2011 Simultaneous measurement of contact angle and surface tension using axisymmetric drop-shape analysis-no apex (adsa-na). *Langmuir* **27** (7), 3485–3495.

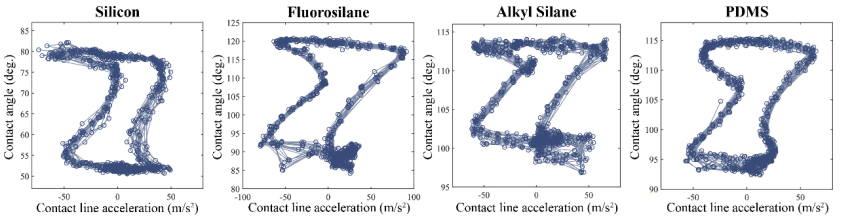

Figure SM 3: The relationship between the dynamic contact angle and contact line acceleration over different surfaces.